Supplementary Figures

Supplementary Figure 1. Characterization of *mDG rtTA*-dependent transactivation patterns of different tetO-linked transgenes

(Corresponds to Main Figure 1)

A) Schematic of genetic strategy to inducibly and reversibly overexpress *Klf-9*. (B) Representative micrographs of *Klf-9* in situ hybridization showing expression in regions quantified in Figure 1D. Within the DG, *Klf9* overexpression and reporter expression was restricted to the granule cell layer (GCL) and absent from mossy cells or hilar interneurons.

C, D) A triple transgenic strategy generates DG-restricted expression. (C) Schematic of triple transgenic design used in D. (D) Sagittal section of triple transgenic *mDG* $^{tetO\text{-}Cre/+;\ floxed\ STOP\ LacZ/+}$ showing DG restricted expression by Beta-Galactosidase staining.

E, F) *mDG* rtTA drives expression of tetO-linked transgenes in forebrain. (E) Schematic of genetic strategy used in F. (F) Representative coronal hemisections showing immunohistochemical labeling for Beta-Galactosidase in *mDG* $^{teto\text{-}TauLacZ/+}$ mice in hippocampus. Scale bars 100μm (B), 500μm (D, F).

Figure S1

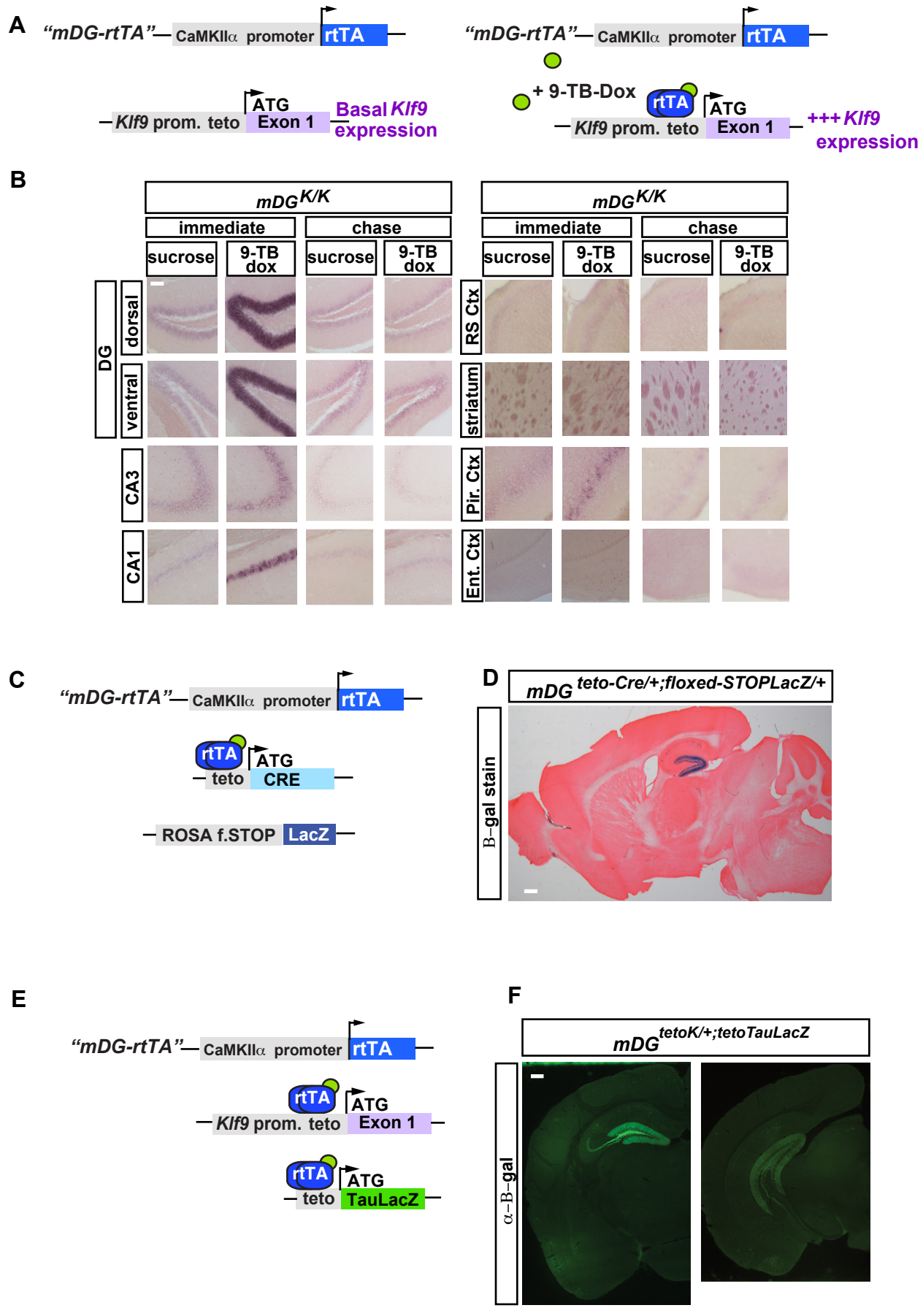
A
"mDG-rtTA"
CaMKIIα promoter
rtTA
Klf9 prom. teto
ATG
Exon 1
Basal Klf9 expression
+ 9-TB-Dox
+++ Klf9 expression
B
mDG K/K
immediate
chase
sucrose
9-TB dox
DG
dorsal
ventral
CA3
CA1
RS Ctx
striatum
Pir. Ctx
Ent. Ctx
C
teto
CRE
ROSA f.STOP
LacZ
D
mDG teto-Cre/+;floxed-STOPLacZ/+
B-gal stain
E
TauLacZ
F
mDG tetoK/+;tetoTauLacZ
α-B-gal

Supplementary Figure 2. Characterization of *c-fos* expression, dendritic spine density in striatum and retrosplenial cortex, and cell death in *mDG* $^{K/K}$ mice (Corresponds to Main Figure 2)

A, B) *mDG* $^{K/K}$ mice show decreased *c-fos* activation in the hippocampus immediately following two weeks of 9TBD treatment in drinking water in A) naïve or B) open field (30 min.) exposed mice (see Figure 2I for quantification).

C,D) At the chase timepoint (two weeks of treatment, followed by two weeks chase) c-fos immunohistochemistry reveals no change in activity in hippocampal regions in 9TBD-treated *mDG* $^{K/K}$ mice that were C) naïve or D) exposed to 30 minutes of open field (see Figure 2J for quantification).

E) *c-fos* activation in striatum of vehicle- and 9-TBD-treated *mDG* $^{K/K}$ mice following 30 minutes of open field exploration at the chase timepoint is similar (n=3,3).

F) *Klf9* overexpression in mature DGCs does not affect IML dendritic spine density. Maximum intensity projection images of confocal z-stack scans of IML dendritic segments of *mDG* $^{K/K;\ Thy1\text{-}GFP/+}$ mice at the immediate timepoint (two weeks of vehicle or 9TBD). Quantification of spine density in the IML (n=4,3, right).

G) 9BTD and vehicle-treated *mDG* $^{K/K}$ mice at chase timepoint have similar dendritic spine densities in AAV_9-CaMKIIα-GFP-labeled striatal neurons or Retrosplenial cortex neurons (n=3,3).

H) Top: representative images of cleaved caspase-3 immunolabled cells in the granule cell layer of 9BTD or vehicle-treated *mDG* $^{K/K}$ mice and wild-type mice 24 hours post-irradiation (tissue kind gift of Dr. David Scadden). Below: Klf9 overexpression does not change the number of dying (cleaved caspase-3+) cells in the DG. Scale bar: 50μm (A-D), 100μm top, 2μm below (F). Data represent mean ± SEM.

Figure S2

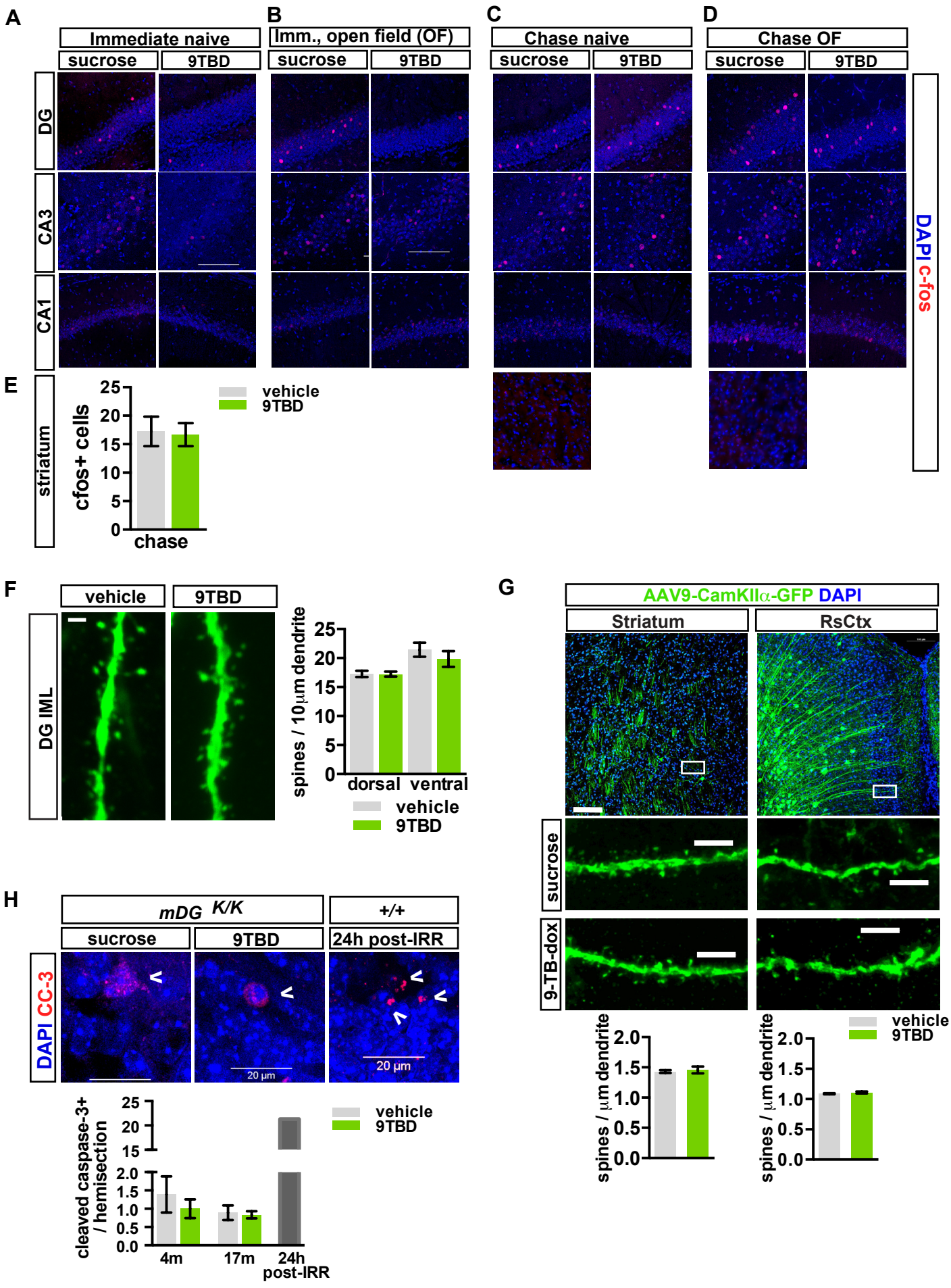
A
Immediate naive
sucrose
9TBD
B
Imm., open field (OF)
sucrose
9TBD
C
Chase naive
sucrose
9TBD
D
Chase OF
sucrose
9TBD
DG
CA3
CA1
DAPI c-fos
E
striatum
cfos+ cells
25
20
15
10
5
0
chase
vehicle
9TBD
F
vehicle
9TBD
DG IML
spines / 10 μm dendrite
25
20
15
10
5
0
dorsal
ventral
vehicle
9TBD
G
AAV9-CamKIIα-GFP DAPI
Striatum
RsCtx
sucrose
9-TB-dox
spines / μm dendrite
2.0
1.5
1.0
0.5
0.0
vehicle
9TBD
H
mDG K/K
+/+
sucrose
9TBD
24h post-IRR
DAPI CC-3
20 μm
cleaved caspase-3+ / hemisection
25
20
15
2.0
1.5
1.0
0.5
0.0
4m
17m
24h post-IRR
vehicle
9TBD

Supplementary Figure 3. Genotype X Treatment enhances adult hippocampal neurogenesis but not olfactory bulb neurogenesis
(Corresponds to Main Figure 3)

A, B) *Klf9* overexpression in mature DGCs affects the survival of adult-born cells of specific ages. Schematic of injection paradigm showing the timing of injection (i.p.) of different thymidine analogs in separate cohorts of *mDG* $^{K/K}$ mice. Representative micrographs of the upper blade of the DG showing BrdU (-3w), CldU (-2w), and IdU (0w) positive cells. (B) Quantification of XdU+ cells per DG: BrdU (-3w, n=4,4, p=0.239), CldU (-2w, n=4,3 p=0.0136), and IdU (0w, n=3,3 p=0.0249).

C, D) Increases in DCX+ numbers and survival of 3 week-old adult-born cells require both genotype (*mDG* $^{K/K}$) and treatment (9TBD). Representative images of BrdU labeling in the upper blade of the DG and DCX labeling in the dorsal DG of *K/K* mice immediately following treatment with sucrose or 9TBD and *mDG* $^{K/K}$ mice treated with 9TBD. (D) Quantification of BrdU positive cells (n=4 [k/k, vehicle], 3 [k/k, 9TBD], 3 [*mDG* $^{K/K}$ 9TBD], ANOVA F=43.58 p<0.0001, k/k vehicle, k/k 9TBD vs. *mDG* $^{K/K}$ 9TBD p<0.05). Quantification of DCX positive cells per dorsal DG section (n=4 [k/k, vehicle], 3 [k/k, 9TBD], 3 [*mDG* $^{K/K}$ 9TBD], ANOVA F=33.66 p<0.0001, k/k vehicle, k/k 9TBD vs. *mDG* $^{K/K}$ 9TBD p<0.05).

E - G) *Klf9* overexpression in *mDG* $^{K/K}$ mice does not affect SVZ neurogenesis. (E) Representative images showing DCX labeling in the SVZ of *K/K* mice and *mDG* $^{K/+}$ mice immediately after two weeks 9TBD treatment. Quantification of DCX+ neurons in SVZ (right, n=4, 3). (E1-E4) Boxes correspond to high magnification images of DCX+ cells in SVZ (E1 and E2) (F) Representative images of proliferation in the SVZ. BrdU labeled cells in the SVZ 2 hours after BrdU injection in *mDG* $^{K/K}$ mice immediately after two weeks treatment with vehicle or 9TBD. Quantification and schematic showing the timing of BrdU injection (right, n=12,10). (G) Images of BrdU positive cells in the MOB of *mDG* $^{K/K}$ mice treated with vehicle or 9TBD. Quantification and schematic showing the timing of BrdU injection (right, n=3,3). Scale bar: 20μm (A), 20μm, 100μm (C), 500μm (E), 500μm (F), 20μm (G). ***p<0.001, **p<0.01, *p<0.05. Data represent mean ± SEM.

Figure S3

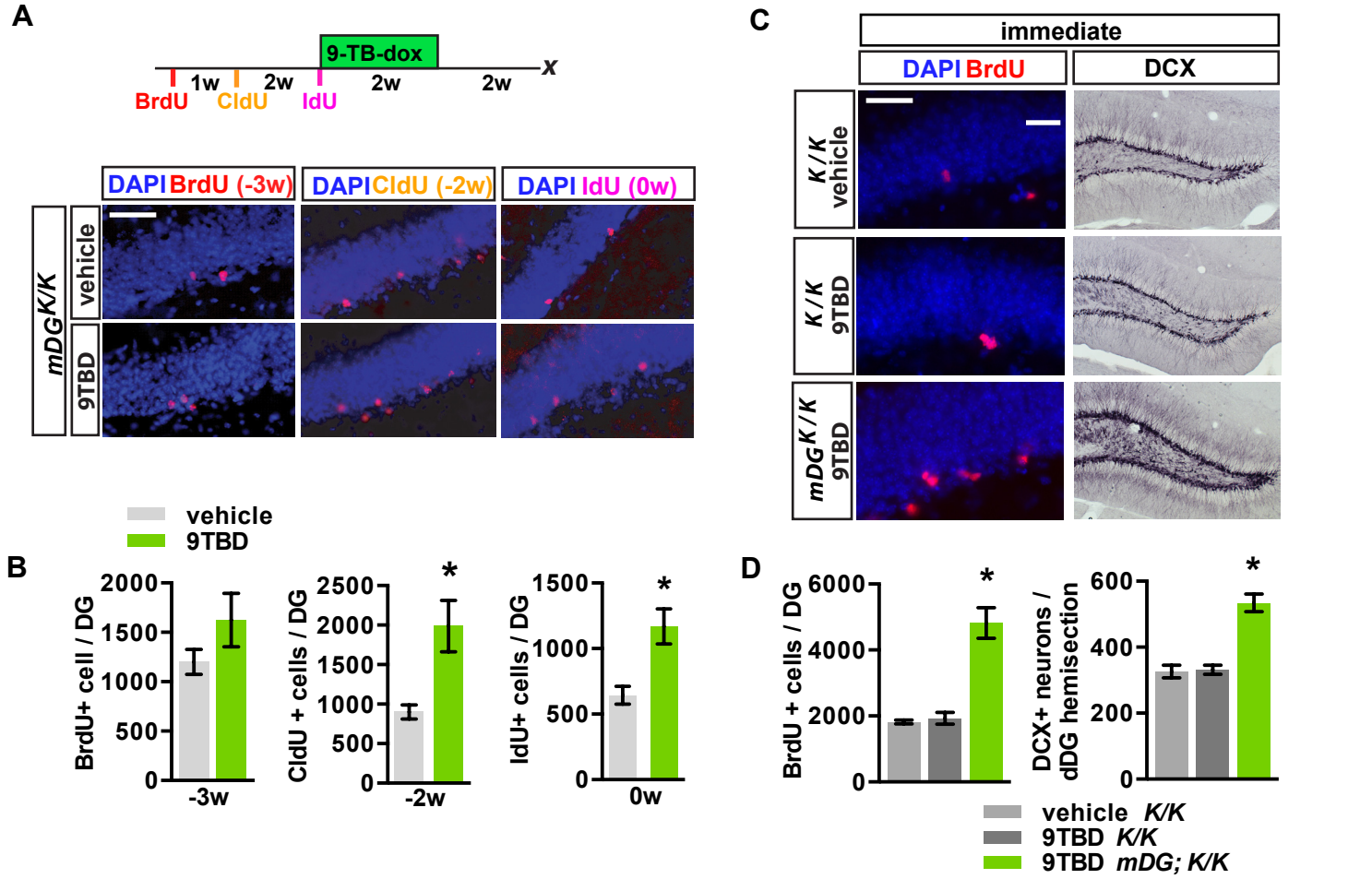
A
9-TB-dox
1w
2w
2w
2w
x
BrdU
CldU
IdU
DAPI BrdU (-3w)
DAPI CldU (-2w)
DAPI IdU (0w)
mDGK/K
vehicle
9TBD
C
immediate
DAPI BrdU
DCX
K/K vehicle
K/K 9TBD
mDGK/K 9TBD
vehicle
9TBD
B
BrdU+ cell / DG
CldU + cells / DG
IdU+ cells / DG
-3w
-2w
0w
D
BrdU + cells / DG
DCX+ neurons / dDG hemisection
vehicle K/K
9TBD K/K
9TBD mDG; K/K
E
DCX
K/K 9TBD
mDG K/+ 9TBD
E1
E2
E3
E4
3 mos.
veh. / 9TBD
2w
SVZ DCX+ cells / hemisection
K/K
mDG K/+
F
SVZ
DAPI BrdU
mDG K/K vehicle
mDG K/K 9TBD
3 mos.
veh. / 9TBD
1w
1w
BrdU
SVZ BrdU+ cells / hemisection
G
MOB
BrdU
3 mos.
veh. / 9TBD
1w
1w
BrdU
2w
BrdU+ cells / image
vehicle
9TBD

Supplementary Figure 4. Analysis of cell fate specification and dendritic complexity, spine density and mossy fiber terminals of adult-born DGCs in *mDG* $^{K/K}$ mice

(Corresponds to Main Figure 5)

A, B) *Klf9* overexpression in mature DGCs does not affect adult-born cell fate specification. (A) Schematic showing timing of BrdU injection and 9TBD administration. Representative confocal images adult-born cells (NeuN+BrdU+, GFAP+BrdU+) in DG. Box indicates image in outlined in gray below. (B) 79.5±5.1% and 85.9±2.4% of 5 week-old BrdU-positive population labeled for NeuN and 5.7±1.7% and 6.1±1.4% labeled for GFAP in vehicle and 9TBD treated mice, respectively.

C-E) *Klf9* overexpression in mature DGCs does not affect adult-born DGC morphology. (C) Schematic showing timing of retroviral injections used in D,E to quantify MFTs from 5 week-old adult-born DGCs labeled with Tdtomato. Representative images of 5 week-old adult-born DGCs and MFTs labeled with TdTomato. (D) MFTs of 5 week-old adult-born DGCs of 9TBD treated *K/K* or *mDG* $^{K/K}$ mice have comparable number of filopodia (n=5,5). Graph displays the percentage of imaged MFTs as function of filopodia number. (E) MFTs of 5 week-old adult-born DGCs of 9TBD treated *K/K* or *mDG* $^{K/K}$ mice are similar in size. Graph displays the percentage distribution of the area of imaged MFTs (n=5,5).

F - I) Scholl analysis reveals that there are no morphological differences between vehicle and 9TBD treated 4-week or 6-week old neurons. (F) Representative maximum intensity projections of Z-stacks of 4 and 6 week old vehicle or 9TBD-treated *mDG* $^{K/K}$ mice. There are no differences in (G) total dendritic length, (H) maximum branch number, or (I) Scholl analysis of branching morphology between 4-week or 6-week-old neurons from vehicle and 9TBD-treated *mDG* $^{K/K}$ mice (n=5 for all groups, with 5-10 neurons per animal). Scale bar: 100μm (A), 500μm, 2 μm below (C). Data represent mean ± SEM.

Figure S4

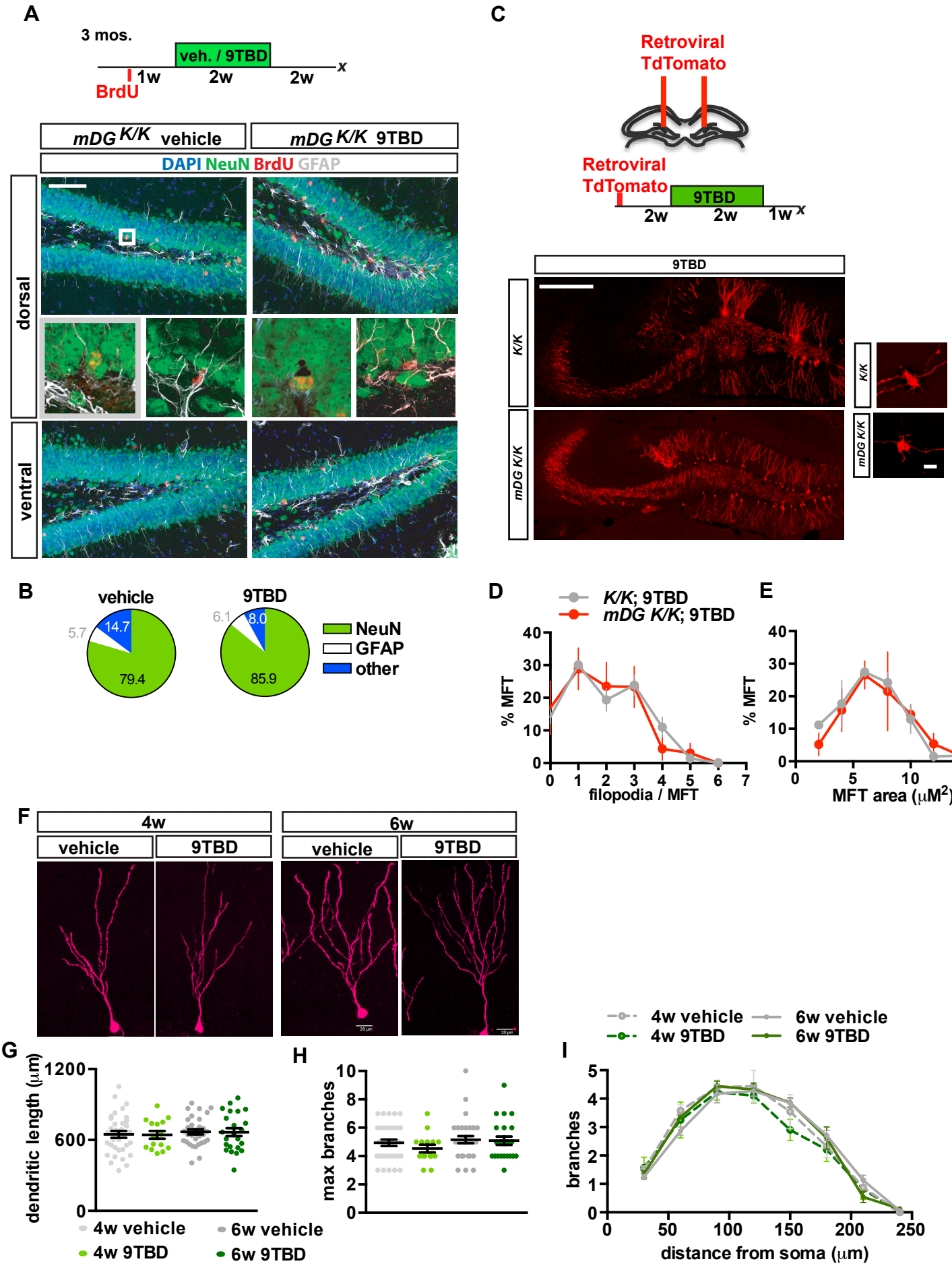
A
3 mos.
veh. / 9TBD
BrdU
1w
2w
2w
x
mDG K/K vehicle
mDG K/K 9TBD
DAPI NeuN BrdU GFAP
dorsal
ventral
C
Retroviral
TdTomato
Retroviral
TdTomato
9TBD
2w
2w
1w
x
9TBD
K/K
mDG K/K
K/K
mDG K/K
B
vehicle
9TBD
5.7
14.7
79.4
6.1
8.0
85.9
NeuN
GFAP
other
D
K/K; 9TBD
mDG K/K; 9TBD
% MFT
filopodia / MFT
E
% MFT
MFT area (μM²)
F
4w
6w
vehicle
9TBD
vehicle
9TBD
G
dendritic length (μm)
4w vehicle
6w vehicle
4w 9TBD
6w 9TBD
H
max branches
I
4w vehicle
6w vehicle
4w 9TBD
6w 9TBD
branches
distance from soma (μm)

Supplementary Figure 5. Genetic expansion of adult-born DGCs or genetic overexpression of *Klf9* in CA1 does not affect innate anxiety and spatial reversal learning, respectively

(Corresponds to Main Figure 6)

A) Schematic of behavioral testing regimen of adult *mDG* $^{K/K}$ mice (n=9, 9 except where indicated).

B) Vehicle and 9TBD treated *mDG* $^{K/K}$ mice exhibited comparable levels of locomotor activity (B') (ANOVA, time: $F_{(11,176)}$=16.78, p<0.0001, treatment: $F_{(1,16)}$=0.005, p=0.9453, interaction: $F_{(11,176)}$=1.187, p=0.2989), rearing behaviors (B'') (p=0.5419), and distance traveled in the periphery or center of the open field (B''') (center, p=0.7339) over 60 minutes.

C) Vehicle and 9TBD treated *mDG* $^{K/K}$ mice traveled comparable distances in the light and dark compartments over 10 minutes (% distance in light, p=0.4712).

D) Vehicle and 9TBD treated *mDG* $^{K/K}$ mice spent comparable time in the open and closed arms of elevated plus maze over 5 minutes (n=14,14 time open arms p=0.2729).

E) Vehicle and 9TBD treated *mDG* $^{K/K}$ mice spent comparable time immobile on day 1 (p=0.6564) and day 2 (p=0.913) of the forced swim test.

F) 9TBD treated *mDG* $^{K/K}$ mice spent more time interacting with the novel object in the test session immediately following three training sessions (n=8,8) (ANOVA, object: $F_{(1,12)}$=7.753, p=0.0165, treatment: $F_{(1,12)}$=10.91, p=0.0063, interaction: $F_{(1,12)}$=1.866, p=0.197).

G) Schematic of behavioral testing regimen of 16 month-old *mDG* $^{K/K}$ mice (n=9,9).

H) Vehicle and 9TBD treated 16 month-old *mDG* $^{K/K}$ mice traveled comparable distances in the light and dark compartments over 10 minutes (% distance in light, p=0.8616).

I) Vehicle and 9TBD treated 16 month-old *mDG* $^{K/K}$ mice exhibited comparable levels of locomotor activity (I) (ANOVA, time: $F_{(11,176)}$=8.519, p<0.0001, treatment: $F_{(1,16)}$=0.3773, p=0.5476, interaction: $F_{(11,176)}$=0.9137, p=0.5285), rearing behaviors (J) (p=0.4540), and distance traveled in the periphery or center of the open field (K) (% distance center, p=0.4289) over 60 minutes.

J - L) Local infusion of 9TBD in *mDG* $^{K/K}$ mice results in CA1-specific overexpression of *Klf9*. (J) schematic of local 9TBD infusion and testing paradigm. (K) Representative images showing CA1 overexpression of KLF9. (L) *Klf9* expression is increased in CA1,

but not DG, following 10 days of local 9TBD infusion (n=3,3, t-test CA1 p=0.0062 DG p=0.5343).

(M - Q) MWM analysis of mice two weeks post-CA1- *Klf9* overexpression reveals no differences in spatial learning, memory, or cognitive flexibility (n=9,9). (M) Both vehicle and 9TBD-treated mice show similar latency to reach the platform and (N) showed similar accurate performance on the initial hidden probe test (ANOVA, vehicle: F=30.07, p<0.0001, target v left, right, opposite p<0.05, 9TBD: F=11.50, p=0.0003, target v left, right, opposite p<0.05). (O) Vehicle and 9TBD-treated mice show no differences in latency to locate the reverse hidden platform location. (P) Both groups failed to prefer the new target quadrant on reversal day 3, whereas (Q) both groups showed a similar accurate preference for the target quadrant on reversal day 5 (ANOVA, vehicle: F=5.054, p=0.0259, target v left, opposite p<0.05, 9TBD: F=4.523, p=0.0488, target v right, opposite p<0.05). *p<0.05. Data represent mean ± SEM.

Figure S5

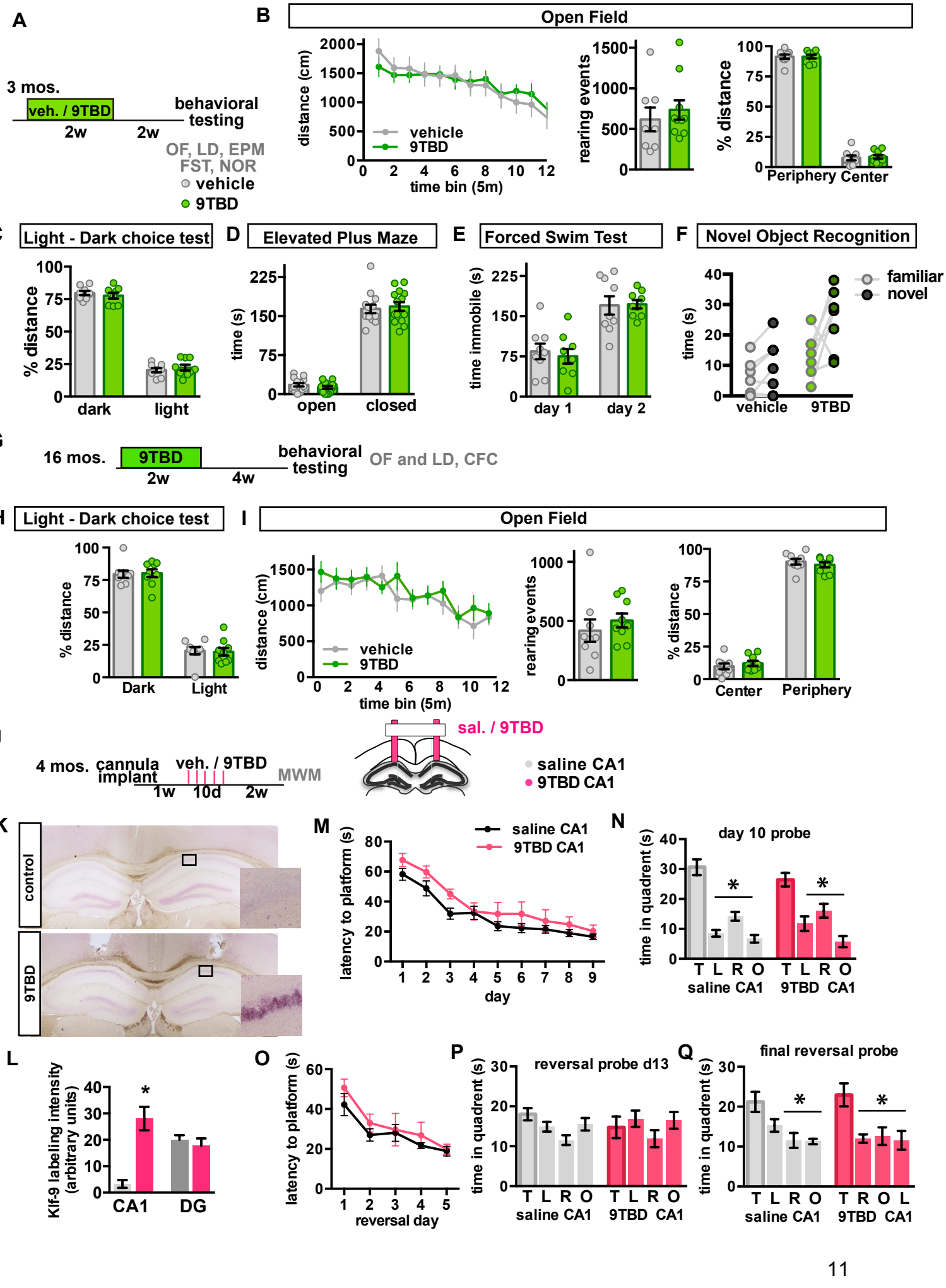
A
3 mos.
veh. / 9TBD
behavioral testing
2w
2w
OF, LD, EPM
FST, NOR
vehicle
9TBD
B
Open Field
distance (cm)
time bin (5m)
vehicle
9TBD
rearing events
% distance
Periphery
Center
C
Light - Dark choice test
% distance
dark
light
D
Elevated Plus Maze
time (s)
open
closed
E
Forced Swim Test
time immobile (s)
day 1
day 2
F
Novel Object Recognition
time (s)
familiar
novel
vehicle
9TBD
G
16 mos.
9TBD
behavioral testing
2w
4w
OF and LD, CFC
H
Light - Dark choice test
% distance
Dark
Light
I
Open Field
distance (cm)
time bin (5m)
vehicle
9TBD
rearing events
% distance
Center
Periphery
J
4 mos.
cannula implant
veh. / 9TBD
MWM
1w
10d
2w
sal. / 9TBD
saline CA1
9TBD CA1
K
control
9TBD
M
saline CA1
9TBD CA1
latency to platform (s)
day
N
day 10 probe
time in quadrent (s)
T L R O
saline CA1
T L R O
9TBD CA1
L
Klf-9 labeling intensity (arbitrary units)
CA1
DG
O
latency to platform (s)
reversal day
P
reversal probe d13
time in quadrent (s)
saline CA1
9TBD CA1
Q
final reversal probe
time in quadrent (s)
saline CA1
9TBD CA1

Supplementary Figure 6. Competence of NSC activation and modulation of neuronal competition dynamics is maintained following reinduction of *Klf9* overexpression in mature DGCs
(Corresponds to Main Figure 7)

A, B) *In situ* hybridization showing that *Klf9* transcripts are upregulated in the DG of 11 month- old *mDG*$^{K/K}$ mice immediately following treatment with 9TBD. (A) Representative images. (B) Quantification of *Klf-9* expression (arbitrary units) in forebrain at the immediate and chase timepoints (n=7 [vehicle], 4 [immediate], 3 [chase], ANOVA, F=19.18 p=0.0005, vehicle vs. 9TBD immediate p<0.05)

C - E) Inducible *Klf9* overexpression in mature DGCs increases proliferation in 11 months old *mDG*$^{K/K}$ mice. (C) Representative Images. (D) Inducible *Klf9* overexpression in mature DGCs increases the Tbr2+ population in 11 months old *mDG*$^{K/K}$ mice (n=3,4, t-test, vehicle vs. dox p<0.0001). (E) Inducible *Klf9* overexpression in mature DGCs increases the MCM2+ population in 11 months old *mDG*$^{K/K}$ mice (n=3,4, t-test vehicle vs. dox immediate, p=0.0112).

F - L) Re-induction of *Klf-9* overexpression. (F) Schematic of experimental design for assessing the impact of re-induction of *Klf9* overexpression in mature DGCs on adult hippocampal neurogenesis in G – L (n=4 [V-V], 3 [D-V], 4[V-D], 4[D-D]). (G) *In situ* hybridization showing that *Klf9* transcripts are upregulated following multiple treatments with 9TBD. (H) Quantification of *Klf-9* expression (arbitrary units) in forebrain following first or second exposure to 9TBD (ANOVA DG: f=18.91 p=0.0002 V-V vs. V-D, D-D p<0.05, CA3: F=5.212 p=0.0201 V-V vs. D-D p<0.05, CA1: F=15.17 p=0.0005 V-V vs. V-D, D-D p<0.05, PC F=6.674 p=0.0094 V-V vs. V-D, D-D p<0.05). (I) Competence of NSC and progenitor activation is maintained following re-induction of *Klf9* overexpression. Representative images of Tbr2, MCM2, and Nestin-MCM2 labeling following first or second exposure to 9TBD. (J) Repeated inducible *Klf9* overexpression in mature DGCs produces comparable increases in the (J) DCX+ population, (K) Tbr2+ (ANOVA F=20.26 p<0.0001, V-V vs. V-D, D-D p<0.05), MCM2+ (ANOVA F=36.11 p<0.0001, V-V vs. V-D, D-D p<0.05) and DCX+ (ANOVA F=23.3 p<0.0001, V-V vs. V-D, D-D p<0.05) populations in the DG, as well as (L) comparable increases in activation of NSCs in the DG (ANOVA F=10.57 p=0.0014, V-V vs. V-D, D-D p<0.05). Scale bar: 500μm (A,G), 20μm (C,I), 50 μm (I, Nestin MCM2) 100μm (J). ***p<0.001, **p<0.01, *p<0.05. Data represent mean ± SEM.

Figure S6

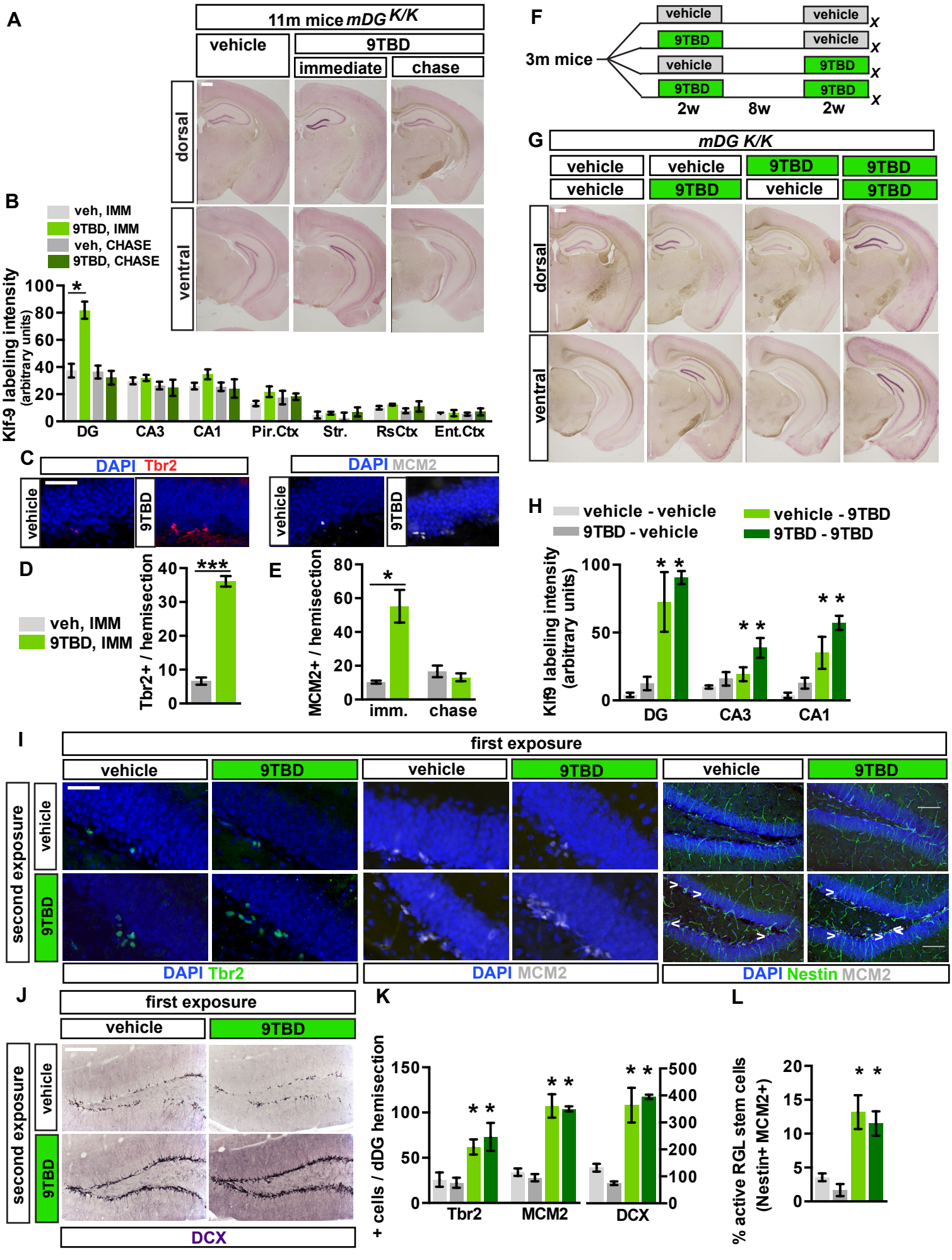
A
11m mice mDG K/K
vehicle
9TBD
immediate
chase
dorsal
ventral
B
veh, IMM
9TBD, IMM
veh, CHASE
9TBD, CHASE
Klf-9 labeling intensity (arbitrary units)
DG
CA3
CA1
Pir.Ctx
Str.
RsCtx
Ent.Ctx
C
DAPI Tbr2
DAPI MCM2
D
Tbr2+ / hemisection
E
MCM2+ / hemisection
imm.
chase
F
3m mice
2w
8w
2w
G
mDG K/K
H
vehicle - vehicle
9TBD - vehicle
vehicle - 9TBD
9TBD - 9TBD
Klf9 labeling intensity (arbitrary units)
I
first exposure
second exposure
DAPI Tbr2
DAPI MCM2
DAPI Nestin MCM2
J
DCX
K
+ cells / dDG hemisection
Tbr2
MCM2
DCX
L
% active RGL stem cells (Nestin+ MCM2+)

Supplementary Figure 7. Representative low magnification images of *c-fos* transcripts localized to nuclear, cytoplasmic, or both compartments in DGCs in response to same, similar or distinct contexts.
(Corresponds to Main Figure 8)

A) Representative confocal images of DG cells exhibiting cytoplasmic, nuclear or nuclear and cytoplasmic localization of *c-fos* transcripts. Scale bar: 50μm.

B) Genetic expansion of a cohort of 5-8 week-old adult-born DGCs decreases reactivation of DG cellular assemblies (A-A: n=6,4 A-B: n= 7,4 A-C: n=7,3, t-test, dorsal [vehicle: A-A vs. A-B p=0.8009, A-C p=0.0391], [9TBD: A-A vs. A-B p=0.0286, A-C p=0.1143]; ventral [vehicle: A-A vs. A-B p=0.2979, A-C p=0.0007]; [9TBD: A-A vs. A-B p=0.0017, A-C p=0.0055]). ***p<0.001, **p<0.01, *p<0.05. Bar graphs represent data as mean ± SEM.

Figure S7

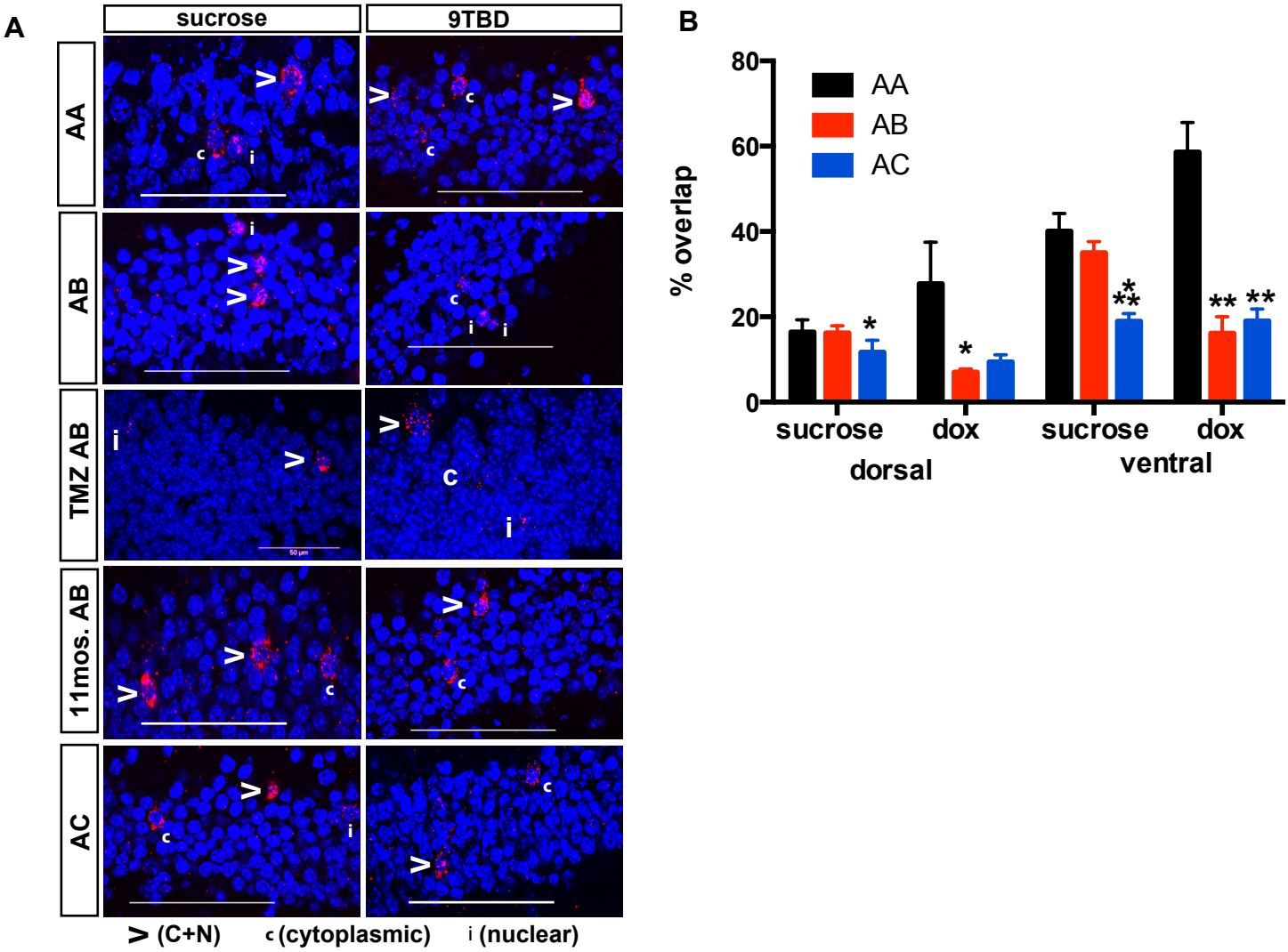
A
sucrose
9TBD
AA
AB
TMZ AB
11mos. AB
AC
> (C+N)
c (cytoplasmic)
i (nuclear)
B
% overlap
AA
AB
AC
sucrose
dox
sucrose
dox
dorsal
ventral

Detailed Methods

Generation of the teto-Klf9 mouse line:

A pGK Neo floxed STOP tetO cassette (Tanaka et al., 2010) was inserted upstream of the translation initiation site (ATG) of *Klf9* gene using standard bacterial artificial chromosome (BAC) recombineering techniques. Germ line-transmitted offspring were established as *Klf-9 Floxed-STOP-tetO* heterozygous knock-in mice (Stop tetO Knock in allele, 8.9Kb band). *Floxed-STOP-tetO* mice were crossed with *ROSA-Flpe mice* (Farley et al., 2000) and FRT sites flanking the Neo-STOP cassette were recombined to generate *TRE-Klf-9* knock in mice (tetO Knock in allele, 6Kb band). Southern Blotting was performed using a 5' probe at 5 kb upstream of the start site (Hind III digest) and a 3' probe 4.5 kb downstream of the start site (Nhe1 digest)(Figure 1A). 6 embryonic stem cells (129 SvEv ES cells, line CSL3) were identified to have undergone the desired gene targeting events. PCR genotyping was performed with a set of primers upstream of the insert and within the PGK Neo sequence, as well as a set of primers within the tetO sequence and downstream of the insert. Arrows in Figure 1A indicate location of primers used for genotyping.

Mouse lines:

The *teto-TauLacZ* reporter line has been described previously (Reijmers et al., 2007) and was purchased from Jackson labs (strain 008344; outcrossed from cfos-tTA). The *teto-Cre* line (Schonig et al., 2002) and inducible Beta galactosidase reporter line *(ROSA fSTOP lacZ)*(Soriano, 1999) have been described previously. The *teto-H2B-GFP* line was obtained from Dr. Konrad Hochedlinger (Foudi et al., 2009). The *teto-SynGFP; TdTomato* line was described previously (Li et al., 2010) and was purchased from Jackson labs (strain 012345). Nestin GFP mice were described previously (Mignone et al., 2004) and were obtained from Dr. David Scadden. *Thy1-GFP* (M Line) mice (Feng et al., 2000) were purchased from Jackson Labs (strain 007788) and were maintained by crossing with $^{K/K}$ or *mDG* $^{K/K}$ mice. *Rac1*$^{f/f}$ conditional mice were previously described (Glogauer et al., 2003) and were purchased from Jackson labs (strain 005550). Tail DNA from all offspring was genotyped by PCR to detect the presence of each transgene separately.

Temozolomide (TMZ) treatment

Briefly, TMZ (Sigma, T2577) was dissolved in DMSO at 25mg/ml, and diluted to 2.5mg/mL in sterile saline. Adult *mDG*$^{K/K}$ mice were given i.p. injections of saline +10% DMSO (vehicle) or TMZ on 3 consecutive days followed by four days with no injections for four weeks. At the start of the third week of dosing, animals were given BrdU via intraperitoneal injection, in 0.9% NaCl at 150mg/kg body weight. Mice did not show overt negative effects of the TMZ treatment and maintained body weight (±10% of starting weight).

Behavioral Experiments

Age-matched, genotyped-matched male *mDG* $^{K/K}$ mice (adult, 3-4 mos., middle-aged 12mos., aged, 17 mos.) were used for all behavioral experiments. Behavioral tasks were performed in the following order: open field (day 1), light-dark choice test (day 2), elevated plus maze (day 3), forced swim test (day 4,5). Novel object recognition, spatial learning and contextual fear conditioning were performed in separate cohorts. For the aged mice, open field and light-dark choice tests were performed prior to CFC. Mice were tested 4 weeks after 9TBD or vehicle treatment.

Open field

Mice were kept in a quiet, darkened room for at least 1 h before the test. Motor activity over 60 min was quantified in four Plexiglas open-field boxes of 41 x 41cm (Kinder Scientific) with 16 sets of double stacked pulse-modulated infrared photobeams equally spaced on every wall (128 total) to record *x–y* ambulatory movements. The software defined grid lines that divided each open field into center and surround regions, with the periphery consisting of the 10cm closest to the wall around the entire perimeter. Dependent measures were the distance traveled in the center, time spent in the center, and distance traveled in the center divided by total distance traveled (percentage distance). Overall motor activity was quantified as the total distance traveled (in centimeters).

Light–dark choice test

The light/dark test was conducted in the open-field chamber as above, but with a dark plastic box that is opaque to visible light but transparent to infrared covering one-half of the chamber area, thus creating dark and light compartments of equal size. An opening at floor level in the center of one wall of the dark compartment allowed passage between

the light and dark compartments. The light compartment was brightly illuminated. Mice were kept in a quiet, darkened room for at least 1 h before the test without food. Between each trial, the whole apparatus was cleaned. At the beginning of the test, the mouse was placed in the dark compartment and allowed to freely explore both compartments for 10 min. Ambulation distance and time spent in the dark and the light compartments were recorded.

Elevated Plus Maze test

The elevated plus maze consisted of black Plexiglass apparatus with four arms (16 cm long and 5 cm wide) set in a cross from a neutral central square (5 cm x 5 cm) placed 1m above the floor. Two opposing arms were delimited by vertical walls (closed arms), while the two other opposing arms had unprotected edges (open arms). Mice were placed in the center and their behavior was recorded for 5 min via a video camera system (ViewPoint, Lyon, France) located above the maze. Cumulative time spent in the open and closed arms, and entries into the open and closed arms, were scored manually by investigators blind to the treatment conditions. An arm visit was recorded when the mouse moved its forepaws into the arm.

Forced-swim test

Mice were placed in transparent plastic buckets (17 cm diameter; 25 cm deep) filled with 23-26°C water for 6 min and the animal's behavior was recorded using an automated video-tracking system. Testing was performed over 2 consecutive days with the first day serving the purpose of pre-exposure. Mobility (swimming and climbing behaviors) on the second day was analyzed using View-Point Life Sciences software.

Novel Object Recognition test

Mice were placed in an arena (45 cm long, 15 cm high and 30 cm wide) with two distinct objects for three sessions (7 minutes each), with a 3 minute intertrial interval. Mice became habituated to the objects during the three training sessions, and one of the objects was then replaced with a novel object in session four. Objects and object positions were counterbalanced during testing. The objects that were selected for testing elicited comparable levels of exploration based on exploration levels in pilot experiments. Sessions were videorecorded, and videos were manually scored for object

exploration (when an animal's snout was 2 cm or less from the object) by an investigator blind to object identity and animal treatment identity.

Contextual Fear conditioning

The contextual fear conditioning protocol (days 1-3) entailed delivery of a single 2 s footshock of 0.7 mA, 180 s after placement of the mouse in the training context. The mouse was taken out 20 s after termination of the footshock. Freezing levels were quantified over the initial 180s prior to the shock. On day 4, animals were exposed to with the training context (in which they did not receive a shock) or a similar context (designated B throughout) for three minutes. 14 and 28 days later, mice were exposed to the training and similar contexts in a counterbalanced design.

Conditioning was conducted in Coulbourn Habitest fear conditioning chambers. with clear front and back Plexiglas walls, aluminum side walls, and stainless-steel bars as a floor. The chamber was lit from above with a light, ventilated with a fan, and encased by a sound-dampening cubicle. On the days of testing, mice were brought out of the vivarium and allowed to habituate for an hour outside the testing room before starting the experiment. Mouse behavior was recorded by digital video cameras mounted above the conditioning chamber. For the training context (designated A throughout), the fan and lights were on, stainless-steel bars were exposed, and ethanol was used as an olfactory cue. Mice were brought into the testing room in a standard housing cage. For B, Mice were brought into the testing room in cardboard buckets. The similar context was modified by covering the stainless-steel bars with a solid floor covered with bedding, and two of the chamber walls were covered using plastic inserts with black and white shapes. Animals were counterbalanced for order of exposure, with the second exposure occurring 1h following the initial test. Exposure to the novel context (designated C throughout), occurred 1h following exposure to the second context. Mice were placed in individual round white cardboard paper chambers inside a large plastic enclosure. Freezeframe and Freezeview software (Actimetrics) were used for recording and analyzing freezing behavior, respectively.

Morris Water Maze and reversal learning

The task was performed with two training phases executed in succession: acquisition phase (9 days, Q3), and reversal phase (reversal learning, 5 days), with a hidden platform in the opposite quadrant (Q1). A probe trial, in which the mice were

released at the center of the opposite quadrent and were allowed to swim for 60 s in the absence of the platform, was performed 24h after the last trial of the acquisition phase (day 10) and twice during the reversal phase (day 13, prior to training, and day 16). The animals' trajectories were recorded with a videotracking system (AnyMaze). The apparatus consisted of a white pool 83cm in diameter and 60cm deep, filled with water to a depth of 29cm. Four black shapes were equally spaced on the walls of the tank as visible cues. Water temperature was maintained at approximately 25°C. A clear Plexiglas goal platform 5cm in diameter was positioned ~0.5cm below the surface of the water (hidden platform), approximately 15 cm from the wall of the tank. Latency to reach the platform and swim speed were recorded for training trials, while swim speed and time in quadrant were calculated for probe trials. Each trial comprised four tests, with mice released facing the wall in the center of each quadrant in a pseudorandom order such that no single start location was used in consecutive tests (10-min intertest interval). Mice were allowed to swim for 90s, and animals that failed to locate the platform in this time were guided to the platform and allowed to rest for 3s before being removed from the tank. 3 trials (~1h intertrial interval) were performed on days 1 - 9, and two trials per day on days 11-15. The average latency to reach the platform was averaged for each trial (4 tests) and for each day. A second cohort of mice (n=9 per group) was tested two weeks after local infusion of 9TBD or saline into CA1.

Cannula implantation and local infusion

Cannula implantation for drug delivery to CA1 was carried out as described previously (Goshen, Cell, 2011). Cannula were purchased from Plastics One (Roanoke, VA) and consisted of bilateral guide cannula (center to center 2.5mm, custom depth 1mm) and removable dummy cannula. Adult (12 - 16 week-old) *mDG* $^{K/K}$ mice were maintained under standard housing conditions, and anaesthetized with ketamine / xylazine (10mg/mL and 1.6mg/mL). Mice were placed in the stereotaxic apparatus and small hole was drilled at each bilateral injection location (anterioposterior = -2mm from bregma; lateral = ±1.25mm) and cannula slowly lowered to the appropriate depth. The cannula was secured to the skull with dental cement. After allowing one week for the mice to recover, the dummy cannula was removed, and the injection cannula was inserted through the guide cannula and projected 0.5mm. The injection cannula was attached to PE50 tubing and a New Era Syringe pump. Saline or 9TBD (dose 10mg /mL, 10µg

infused in 1µl) was infused at a rate of 1µl / minute on each side sequentially to ensure equal delivery. Drug or vehicle was infused every other day for 10 days (5 injections).

Retroviral / Rabies virus / AAV injections

For all surgeries, mice were given carbofen (5mg/kg body weight subcutaneous in sterile saline) prior to surgery and 24h later to minimize discomfort.

Retroviral infection: Briefly, stable human 293-derived gpg retroviral packaging cell line (kindly provided by S. Ge, Stony Brook University School of Medicine, NY) was co-transfected with retroviral plasmids expressing TdTomato (generous gift of Dr. Shaoyu Ge) and pVSVG. Virus-containing supernatant was harvested 36, 48, and 60 h after transfection and concentrated by ultracentrifugation at 25,000 rpm for 1.5 h. Adult (6 - 8 week- old) *mDG* $^{K/K}$ mice and $^{K/K}$ littermates were maintained under standard housing conditions, and anaesthetized with ketamine / xylazine (10mg/mL and 1.6mg/mL). Mice were placed in the stereotaxic apparatus and small hole was drilled at each bilateral injection location and injected with 1µl virus per site injected using a Hamilton microsyringe (0.1 µl/min) into the dorsal DG using the following coordinates: anterioposterior = −2 mm from bregma; lateral = ± 1.6 mm; ventral = 2.5 mm. The skin incision was closed carefully after retroviral injection to minimize inflammation. Injection needles were left in place for 10 min after injection to ensure even distribution of the virus. Mice were sacrificed 5 weeks post infection to examine mossy fiber terminal (MFT) connectivity of TdTomato+ adult-born neurons. (See Figure S4C for timeline.)

Rabies virus: The retrovirus CAG-DsRedExpress2-2A-G-IRES2-TVA, encoding DsRedExpress2, the RABV glycoprotein (G), and TVA800 (the GPI anchored form of the TVA receptor), designed as retro-DsRed-G-TVA, was described previously (Deshpande et al., 2013, Begami, 2015). This plasmid was used to transfect the 293-derived gpg retroviral packaging cell line as described above, except virus was harvested at 2, 4, and 6 days after transfection, followed by ultracentrifugation to concentrate the virus. Construction and amplification of the G gene-deleted GFP-expressing RABV (SADDG-GFP, here designated RABVΔG) have been described previously (Wickersham et al., 2007a; Wickersham et al., 2007b; Bergami et al., 2015). Bilateral dorsal DG stereotaxic injections of retro-DsRed-G-TVA in *mDG* $^{K/K}$ mice were carried out as described above. Psuedotyped rabies virus was injected at the same stereotaxic coordinates, three or five weeks following starter virus retroviral infection. For the 4 week cohort, mice were treated with vehicle or 9TBD for 14 days starting at 3 days post-retroviral injection,

injected with RABVΔG four days after the end of treatment, and sacrificed 1 week later (to allow expression and propagation of RABVΔG). For the 6 week cohort, mice were treated with vehicle or 9TBD for 14 days starting at 1 week post-retroviral injection, injected with RABVΔG 2 weeks after the end of treatment, and sacrificed 1 week later (See timeline in Figure 5E). Connectivity ratios were computed as (traced cells, GFP+)/ (starter cells, GFP+DsRed+).

AAV: For injection analysis of dendritic spine density in striatum and retrosplenial cortex, AAV_9-CaMKinaseIIα-GFP virus was purchased from the University of Pennsylvania virus core (titre $6.27x10^{13}$). Virus was diluted 1:50 to allow sparse infection, and 0.1 µl (0.05 µl/min) injected in the striatum (anterioposterior = +1mm from bregma; lateral = -1.9mm; ventral = -3.2 mm from skull surface) and retrosplenial cortex (anterioposterior = -1.6mm from bregma; lateral = ±0.5mm; ventral = -1.3mm from skull surface) using the anaesthetization protocol described above. Mice were treated with vehicle or 9TBD for 14 days starting at 3 days post-surgery, and sacrificed 2 weeks following the end of treatment.

Rac1: Viruses were diluted (below) to ensure local infection of the Cre virus and very sparse labeling with eYFP to facilitate spine analysis. To control for virus, floxed/floxed and wildtype littermates were injected with Cre/ DIO eYFP viruses (1:100 CRE + 1:500 DIO-eYFP). (University of Pennsylvania virus core, Cre titre $1.07x10^{13}$, University of North Carolina virus core, DIO-eYFP titre $5.87x10^{12}$). To control for genotype, floxed/floxed mice were injected with AAV_9-CaMKinaseIIα-GFP virus + AAV_5-EF1α–DIO-eYFP (1:50 DIO-eYFP + 1:1000 GFP) viruses (University of Pennsylvania virus core, GFP titre $6.27x10^{13}$). Equal total viral particles were injected for each group. 0.2µl (0.05 µl/min) of virus cocktail was injected in the molecular layer of the DG (from bregma: anterioposterior = -2mm; lateral = +1.4mm; ventral = -2.1mm from skull surface) using the anaesthetization protocol described above.

Sholl analysis of 4 and 6-week-old neurons

A Nikon A1R Si confocal laser, a TiE inverted research microscope, and NIS Elements software were used to capture z-stacks for Scholl analysis using a 20x objective. Images were acquired as 30 µM Zstacks with a step size of 2.5 µM. Images of collapsed z-stacks were using the tracing tool in NIS Elements. Dendritic complexity was analysed using the Sholl analysis tool in NIS Elements. The centre of all concentric circles was placed at the centre of the cell's soma. The parameters used were starting radius (30

μm), ending radius (250 μm from the centre) and interval between consecutive radii (30 μm). Total branch number was counted manually, as were the number of branch intersections at each distance from the soma by an investigator blind to experimental conditions.

Image analysis of mossy fiber terminals

A Nikon A1R Si confocal laser, a TiE inverted research microscope, and NIS Elements software were used to capture z-stacks for Mossy fiber terminal (MFT) imaging using a 60x objective as we recently published (Ikrar et al., 2013). Images were acquired as 15 μM Zstacks with a step size of 0.5 μM. Area of individual MFTs was assessed at the widest point in the Z-stack using Image J MaxEntropy thresholding, followed by unbiased area selection with the tracing tool. MFTs area was analysed for >50 individual MFTs per mouse (702 total) to calculate the cumulative percentage of terminals at each size or smaller.

Image analysis of dendritic spines

For quantification of dendritic spines, confocal z-stack images were acquired using a Nikon A1R Si confocal laser, a TiE inverted research microscope, and NIS Elements software. Imaging was performed using a 60x objective, plus 1.5x optical zoom and 6x digital zoom. For spine imaging, confocal 2.1uM z-stacks (2048 resolution) with 0.3uM step size were taken centered on dendritic segment. Z-stacks were flattened using the maximum intensity projection, and flattened images were quantified using image J. For spine density, spines were counted manually for at least 80uM of dendritic length per region per mouse. The Edge fitter plugin (www.ghoshlab.org) was used to measure head diameter (at the widest point of the spine head) while length was measured manually from dendrite to the furthest point of the spine head. >150 spines were analyzed per region per mouse to calculate spine size distribution (4,538 DG and 5,138 CA1 spines from 14 mice). The outer molecular layer was defined as the 1/3 of the molecular layer furthest from the granule cell layer, while the inner molecular layer was defined as the 1/3 of the dendritic tree closest to the granule cell layer. Stratum radiatum was defined as the 2/3 of the dendritic tree ventral to the pyramidal layer. For quantification of spines containing PSD95, confocal 2.1uM z-stacks (2048 resolution) with 0.3μM step size were taken centered on dendritic segment. Spines were considered

positive for PSD95 if PSD95 labeling overlapped with the GFP+ spine head in any plane. All imaging and quantification were performed by an investigator blind to treatment.

Immunohistochemistry

Sections were stored in PBS with 0.01% sodium azide at 4°C. For BrdU, CldU/ IdU, CldU/ GFP, MCM2, MCM2/ GFP, MCM2/ Nestin/ Tbr2, and BrdU / GFAP / NeuN immunohistochemistry, sections (1 set) were mounted onto SuperFrost Plus charged glass slides. Sections were subjected to antigen retrieval in 10 mM citrate buffer (pH 6) using a boiling protocol. After cooling to room temperature, sections were rinsed three times in PBS and blocked in PBS with 0.3% Triton X-100 and 10% normal donkey serum (NDS) for 2 h at room temperature. Incubation with primary antibodies (rat anti-BrdU 1:100 dilution, Serotec; mouse anti-MCM2 1:500, BD Biosciences; chicken anti-Nestin 1:500, Aves; rabbit anti-Tbr2, 1:500, Abcam; mouse anti-NeuN 1:500, Chemicon; Rabbit anti-GFAP, 1:1000 DAKO) was carried out at 4°C overnight. Fluorescent-label-coupled secondary antibodies (Jackson ImmunoResearch) were used at a final concentration of 1:300 in PBS:glycerol.

For assessment of neuronal age in *mDG* $^{K/+;\ teto\ H2BGFP/+}$ mice injected with CldU/IdU, antigen retrieval was carried as described for BrdU labeling above. Rat ant-BrdU (Accurate Chemicals, 1:500, recognizes CldU but not IdU) and mouse anti-BrdU (BD Biosciences, 1:50, recognizes IdU but not CldU) were used as described previously (Stone et al., 2011) along with anti-GFP (rabbit, 1:1000, Life Technologies). 303 XdU+ cells were analyzed for three mice. For assessment of neuronal age in *mDG* $^{K/+;\ teto\ H2BGFP/+}$ mice, *mDG* $^{K/+;\ teto\ TauLacZ/+}$ mice, and *mDG* $^{K/+;\ tetoTdTomato/+}$ mice, floating sections were labeled for GFP (rabbit, 1:1000, Life Technologies and DCX (Santa Cruz, goat, 1:500), β-galactosidease (chicken, 1:1000, Abcam) and DCX, or DsRed (rabbit, 1:1000, Clontech) and DCX respectively using the same protocol as used for cfos. 2320 cells were counted from 9 mice of three genotypes. To assess the age of GFP expressing cells in *mDG*$^{K/K;Thy\text{-}1GFP}$ mice, CldU and GFP labeling was carried out as described for BrdU. 187 cells were counted from three mice.

To assess stem cell activation, sections from *mDG* $^{K/K}$ mice were double-labeled for Nestin and MCM2 as described above. In addition, sections from *mDG* $^{K/K;\ Nestin\ GFP+}$ mice were double-labeled for GFP and MCM2 as described above. Confocal stacks (1024 resolution, 2μM step size, 24 μM z-stack) were taken through 3-6 dorsal DG hemisections per mouse. Activated stem cells were defined as Nestin+ cells (or GFP+

cells) with radial glial-like morphology that showed colocalization of MCM2. Nestin+MCM2+ (or GFP+ MCM2+) were counted and quantified as a percentage of the total Nestin+ (or GFP+) population with radial glial-like morphology.

For DCX immunohistochemistry, floating sections were first quenched to remove endogenous peroxidase activity (with 1% H2O2 in 1:1 PBS:methanol). Sections were then washed in PBS, blocked (in PBS containing 0.3% Triton X-100 and 10% NDS) and incubated with primary antibody overnight at 4 °C (DCX, goat, 1:2000, SantaCruz Biotechnology). Following washes in PBS, sections were incubated with horse-radish-peroxidase-coupled, biotinylated secondary antibodies for 2h. Following incubation with ABC solution (Vector Labs) for 1h, the color reaction was carried out using a DAB kit (Vector Labs). X-Gal staining for ß-galactosidase activity was performed as previously described (Schonig et al., 2002)

For BrdU, Tbr2, MCM2, and DCX analysis, positive cells in the granule cell layer and sub-granule zone were counted manually along the dorsal to ventral axis of the DG (1 set of 6; 9 sections). Summing the counted cells and multiplying by 6 yields the total per animal. For c-fos analysis, positive cells in the granule cell layer and CA3 or CA1 (cfos) pyramidal layer were counted manually along the dorsal to ventral axis of the hippocampus (1 set of 6; 3 sections each dorsal, intermediate, and ventral regions).

For assessing neurogenesis in the SVZ, matched sections were compared throughout the dorsal to ventral extent of the SVZ according to the Paxinos and Franklin atlas. DCX positive cells at the border of the ventricular zone were counted manually per hemisection. In a separate cohort of mice, proliferation in the SVZ was assessed by counting SVZ BrdU positive cells (2 hours post-injection of BrdU). Survival of SVZ generated neurons was assessed by counting BrdU-positive neurons in the granule layer in the MOB.

To label c-fos (rabbit, Calbiochem, 1:10,000) and Cleaved caspase-3 (Cell Signaling, rabbit, 1:500) floating sections were used. Briefly, sections were washed in PBS, blocked in PBS buffer containing 0.3% Triton X-100 and 10% NDS, and incubated in primary antibodies overnight with shaking at 4 °C. The next day, sections were washed three times in PBS and incubated with fluorescent-label-coupled secondary antibodies (Jackson ImmunoResearch) for 2 h at room temperature. Data shown as cells per hemisection. For PSD95 / GFP / VGlut1 labeling, sections were labeled as for c-fos, except PBS with 0.5% Triton X-100 was used in place of the 0.3% Triton X-100. The PSD95 antibody was developed by / obtained from the UC Davis/ NIH NeuroMab

Facility (clone K28/43 mouse, 1:500). Primary antibodies VGlut-1 (Synaptic Systems, guinea pig, 1:2000), GFP (Novus, goat, 1:500).

All analysis was performed by an investigator blinded to treatment and/or genotype. Dorsal and ventral sections were defined according to the Paxinos and Franklin (1997) atlas (dorsal Bregma -0.9 to -2.1; ventral Bregma -2.7 to -3.88).

In situ hybridization

In situ hybridization (ISH) was performed using dioxygenin-labeled riboprobes on 35µm cryosections generated from perfused tissue as described previously (Scobie et al., 2009). Premixed RNA labeling nucleotide mixes containing digoxigenin-labled UTP (Roche Molecular Biochemicals) were used to generate RNA riboprobes. Riboprobes were purified on G-50 Microspin columns (GE Healthcare). Probe concentration was confirmed by Nanodrop. Briefly, sections were mounted on charged glass (Superfrost Plus) slides and postfixed for in 4% paraformaldehyde (PFA). Sections were then washed in DEPC-treated PBS, treated with proteinase K (40 µg/ml final), washed again in DEPC-treated PBS, and then acetylated. Following prehybridization, sections were incubated with riboprobe overnight at 58°, washed in decreasing concentrations of SSC buffer, and immunological detection was carried out with anti-Dioxygenin antibody conjugated with alkaline phosphatase. Color reaction was carried out with NBT/BCIP. Color reaction times were identical for both treatment groups. For quantification, 2-4 color images per region per mouse were analyzed using the mean intensity function in Image J. All images were captured using the same light intensity and exposure times. The mean intensity of the region of interest (minus mean intensity of a selected background region) was averaged across images for each mouse and each treatment group.

catFISH: Riboprobes were prepared as for Klf9. Coronal brain sections (20 µm) were prepared using a cryostat and representative series of dorsal and ventral hippocampal sections were organized on slides (Superfrost Plus, VWR) and stored at –80°C until use. Sections were fixed in 4% buffered paraformaldehyde, treated with 0.5% acetic anhydride/1.5% triethanolamine, and incubated in acetone:methanol, equilibrated in 2xSSC before equilibration in prehybridization solution for 1h. Riboprobes were diluted to (2.5ng /µl; 150 µl per slide) in hybridization buffer, heat denatured, chilled on ice, and then added to each slide. Coverslips were added to the slides, and hybridization was carried out at 65°C for 16 hours. Slides were washed in decreasing concentrations of

SSC, including a wash at 37°C in 2x SSC with RNase A (10 µg per ml), and a final wash in 0.5xSSC at 55°C. Endogenous peroxidase activity was quenched with 2% H202 in SSC, slides were blocked (with blocking agent from the DirectFISH kit [NEN Life Sciences, Boston, Massachusetts] plus 5% sheep serum and 0.1% Tween-20), and incubated with horseradish peroxidase (HRP)-antibody conjugate (0.16 µg per ml; Jackson Immunoresearch) overnight at 4°C. Slides were washed three times in Tris-buffered saline (with 0.05% Tween-20), and then a 1:50 dilution of the CY3-tyramine substrate (Perkin Elmer) was added for 30m at RT. Slides were washed three times in Tris-buffered saline (with 0.05% Tween-20) and coverslipped with mounting media containing DAPI (Fluoromount with DAPI, Southern Biotech). Confocal z-stack images using a 60x objective (0.75 µm step size) were acquired along the DG GCL using a Nikon A1R Si confocal laser, a TiE inverted research microscope, and NIS Elements software. Image analysis was performed with NIS Elements software. Four to eight hemisections were scanned per mouse. Images were manually counted for *c-fos* labeling. For analysis of global remapping using catFISH, the exposure paradigms utilized the training context associated with a foot-shock (context A) and exposure to a similar context (high interference, context B), or distinct context (low interference, context C), or re-exposure to the training context. Quantification was performed by an investigator blind to treatment condition.

Statistical Analysis

Statistical analysis was carried out using GraphPad Prism software. Unpaired two-tailed Student's t-tests were used to compare two groups. *, $P<0.05$. To compare groups across training days for the morris water maze and contextual fear conditioning, two-way repeated measures ANOVA was used. For the morris water maze probe test analysis, one-way ANOVA was performed for each group to compare preference for each quadrant. For contextual fear conditioning, behavioral data were scored by two experimenters, including one unrelated to the project. Spine head diameter distribution and mossy fiber terminal size distribution were assessed using Komolgrov-Smirnov tests with significance at $p<0.001$. Spearman's rank-order correlation analysis was performed to analyze the relationship between spine density and DCX+ population.

Supplementary References

Bergami, M., Masserdotti, G., Temprana, S.G., Motori, E., Eriksson, T.M., Gobel, J., Yang, S.M., Conzelmann, K.K., Schinder, A.F., Gotz, M.*, et al.* (2015). A critical period for experience-dependent remodeling of adult-born neuron connectivity. Neuron *85*, 710-717.

Farley, F.W., Soriano, P., Steffen, L.S., and Dymecki, S.M. (2000). Widespread recombinase expression using FLPeR (flipper) mice. Genesis *28*, 106-110.

Feng, G., Mellor, R.H., Bernstein, M., Keller-Peck, C., Nguyen, Q.T., Wallace, M., Nerbonne, J.M., Lichtman, J.W., and Sanes, J.R. (2000). Imaging neuronal subsets in transgenic mice expressing multiple spectral variants of GFP. Neuron *28*, 41-51.

Foudi, A., Hochedlinger, K., Van Buren, D., Schindler, J.W., Jaenisch, R., Carey, V., and Hock, H. (2009). Analysis of histone 2B-GFP retention reveals slowly cycling hematopoietic stem cells. Nature biotechnology *27*, 84-90.

Glogauer, M., Marchal, C.C., Zhu, F., Worku, A., Clausen, B.E., Foerster, I., Marks, P., Downey, G.P., Dinauer, M., and Kwiatkowski, D.J. (2003). Rac1 deletion in mouse neutrophils has selective effects on neutrophil functions. J Immunol *170*, 5652-5657.

Ikrar, T., Guo, N., He, K., Besnard, A., Levinson, S., Hill, A., Lee, H.K., Hen, R., Xu, X., and Sahay, A. (2013). Adult neurogenesis modifies excitability of the dentate gyrus. Frontiers in neural circuits *7*, 204.

Li, L., Tasic, B., Micheva, K.D., Ivanov, V.M., Spletter, M.L., Smith, S.J., and Luo, L. (2010). Visualizing the distribution of synapses from individual neurons in the mouse brain. PLoS ONE *5*, e11503.

Mignone, J.L., Kukekov, V., Chiang, A.S., Steindler, D., and Enikolopov, G. (2004). Neural stem and progenitor cells in nestin-GFP transgenic mice. J Comp Neurol *469*, 311-324.

Reijmers, L.G., Perkins, B.L., Matsuo, N., and Mayford, M. (2007). Localization of a stable neural correlate of associative memory. Science *317*, 1230-1233.

Schonig, K., Schwenk, F., Rajewsky, K., and Bujard, H. (2002). Stringent doxycycline dependent control of CRE recombinase in vivo. Nucleic Acids Res *30*, e134.

Scobie, K.N., Hall, B.J., Wilke, S.A., Klemenhagen, K.C., Fujii-Kuriyama, Y., Ghosh, A., Hen, R., and Sahay, A. (2009). Kruppel-like factor 9 is necessary for late-phase neuronal maturation in the developing dentate gyrus and during adult hippocampal neurogenesis. J Neurosci *29*, 9875-9887.

Soriano, P. (1999). Generalized lacZ expression with the ROSA26 Cre reporter strain. Nat Genet *21*, 70-71.

Stone, S.S., Teixeira, C.M., Zaslavsky, K., Wheeler, A.L., Martinez-Canabal, A., Wang, A.H., Sakaguchi, M., Lozano, A.M., and Frankland, P.W. (2011). Functional convergence of developmentally and adult-generated granule cells in dentate gyrus circuits supporting hippocampus-dependent memory. Hippocampus *21*, 1348-1362.

Tanaka, K.F., Ahmari, S.E., Leonardo, E.D., Richardson-Jones, J.W., Budreck, E.C., Scheiffele, P., Sugio, S., Inamura, N., Ikenaka, K., and Hen, R. (2010). Flexible Accelerated STOP Tetracycline Operator-knockin (FAST): a versatile and efficient new gene modulating system. Biol Psychiatry *67*, 770-773.

Wickersham, I.R., Finke, S., Conzelmann, K.K., and Callaway, E.M. (2007a). Retrograde neuronal tracing with a deletion-mutant rabies virus. Nature methods *4*, 47-49.

Wickersham, I.R., Lyon, D.C., Barnard, R.J., Mori, T., Finke, S., Conzelmann, K.K., Young, J.A., and Callaway, E.M. (2007b). Monosynaptic restriction of transsynaptic tracing from single, genetically targeted neurons. Neuron *53*, 639-647.